INTERNATIONAL JOURNAL OF REFRIGERATION 49 (2015) 169–182

Available online at www.sciencedirect.com

ScienceDirect

journal homepage: www.elsevier.com/locate/ijrefrig

Transient modeling of a flash tank vapor injection heat pump system – Part I: Model development

Hongtao Qiao[*], *Vikrant Aute*, *Reinhard Radermacher*

Center for Environmental Energy Engineering, University of Maryland, College Park, 4164 Glenn L. Martin Hall Bldg., MD 20742, USA

ARTICLE INFO

Article history:
Available online 19 July 2014

Keywords:
Transient
Modeling
Vapor injection
Two-phase flow
Flash tank
Modelica

ABSTRACT

This two-part article explores the dynamic behavior of a flash tank vapor injection heat pump system from a numerical simulation perspective. Part I provides a first-principles model describing the transient heat transfer and flow phenomena of the system with detailed modeling techniques for each component. The vapor injection scroll compressor is analyzed with the internal heat transfer between the refrigerant and metallic parts taken into account. Lumped-parameter models are developed for the flash tank and expansion devices. Heat exchangers are modeled using a finite volume approach and accounting for the complex tube circuitry. The separated flow model without interfacial exchange is utilized for two-phase flows in order to incorporate an appropriate void fraction model so that a more accurate prediction for refrigerant mass distribution can be achieved. The modular nature of the component models allows flexibility in the system configuration. Transient simulations are carried out for start-up and shut-down operations. A detailed comparison of model predictions against experimental data is presented in the companion paper.

Modélisation transitoire d'un systéme de pompe à chaleur à injection de vapeur à partir d'un réservoir à vaporisation instantanée – Partie I: développement du modéle

Mots clés : Transitoire ; Modélisation ; Injection de vapeur ; Ecoulement diphasique ; Réservoir intermédiaire ; Modelica

1. Introduction

Flash tank vapor injection (FTVI) system has been gaining popularity since it was first introduced to the market in late 1970s (Umezu and Suma, 1984). Its applications have increased considerably in order to satisfy various needs, such as heating, cooling and refrigeration (Baek et al., 2008; Cho et al., 2009; Scarcella and Chen, 2010). Compared to the conventional systems without vapor injection, FTVI systems are operated under lower discharge temperatures and have higher performance in energy efficiency. Moreover, these systems are able to adjust the capacity by altering the vapor injection ratio (Winandy and Lebrun, 2002). Experimental

* *Corresponding author*. Tel.: +1 301 405 7314.
E-mail address: htqiao@umd.edu (H. Qiao).
http://dx.doi.org/10.1016/j.ijrefrig.2014.06.019
0140-7007/

Nomenclature

Symbols

a_1–a_3	curve fitting constants [-]
A	area [m^2]
b_1–b_5	curve fitting constants [-]
c_0–c_3	curve fitting constants [-]
c_p	specific heat [J kg^{-1} K^{-1}]
C_v	discharge coefficient [-]
d	diameter [m]
e_{sh}	error between the measured superheat and the set point [K]
f	pressure drop coefficient [-]
F	spring force [N]
G	mass flux [kg m^{-2}]
h	enthalpy [J kg^{-1}]
$\overline{h}$	mass flow weighted enthalpy [J kg^{-1}]
$\overline{h}_{FT}$	mass-based refrigerant mean enthalpy in flash tank [J kg^{-1}]
$\overline{h}_{\rho}$	density weighted enthalpy [J kg^{-1}]
H	height [m]
K	PID gain [-]
Le	Lewis number [-]
$\dot{m}$	mass flow rate [kg s^{-1}]
M	mass [kg]
n	polytropic index [-]
N	motor speed [min^{-1}]
p	pressure [N m^{-2}]
P	perimeter [m]
q	heat transfer rate [W]
q''	heat flux [W m^{-2}]
R	thermal resistance [K W^{-1}]
t	time [s]
T	temperature [K]
u	velocity [m s^{-1}]
V	volume [m^3]
$\dot{V}$	volumetric flow rate [m^3 s^{-1}]
$\dot{W}$	power [W]
x	flow quality [-]
$\hat{x}$	static quality [-]
y	spring deflection [m]
Δ	difference
Δy	segment length along the direction of air flow [m]
Δz	segment length along the direction of refrigerant flow [m]

Greek letters

α	heat transfer coefficient [W m^{-2} K^{-1}] or mass transfer coefficient [kg s^{-1} m^{-2}]
β	angle [degree]
ε	emissivity [-]
γ	void fraction [-]
η	efficiency [-]
φ	valve opening fraction [-]
κ	spring constant [N m^{-1}]
μ	dynamic viscosity [kg m^{-1} s^{-1}]
ρ	density [kg m^{-3}]
σ	Boltzmann constant [m^2 kg^2 s^{-2} K^{-1}]
τ	time constant [s] or wall shear stress [N m^{-1}]
ω	humidity ratio [kg H_2O/kg dry air]
ξ_{shf}	fraction of mechanical loss at the shaft [-]
ζ	built-in volume ratio of the first stage [-]

Subscripts

a	air
als	between ambient and compressor lower-shell
amb	ambient
aus	between ambient and compressor upper-shell
b	sensor bulb of TXV
c	correction
comp	compression
cs	cold stream
d	derivative
diaph	diaphragm of TXV
dis	discharge
disp	displacement
eo	evaporator outlet
eq	equalization
exp	expansion device
f	saturated liquid
face	frontal face
fg	liquid to gas
fin	fin
FT	flash tank
g	saturated vapor
h	mass flow weighted
hcs	between hot stream and cold stream
hs	hot stream
i	integral
in	inlet
inj	injected flow
int	intermediate stage
liq	liquid
lo	liquid outlet
ls	compressor lower-shell
m	motor or mass transfer
max	maximum
mech	mechanical
mix	mixing
nom	nominal
o	external
offset	offset
ori	orifice of TXV
out	outlet
p	proportional
pin	pin of TXV
r	refrigerant
rated	rating conditioning
rev	reversing valve
rls	between refrigerant and compressor lower-shell
rm	between refrigerant and compressor motor
rscr	between refrigerant and compressor scroll set
rshf	between refrigerant and compressor shaft
sat	saturation
scr	scroll set
sh	superheat

shf	shaft	vo	vapor outlet
suc	suction	w	wall
t	tube	ρ	density weighted
target	target	1	suction chamber control volume
tot	total	2	economizer port control volume
us	compressor upper-shell	3	after the compression process
vap	vapor	4	discharge port control volume

studies (Table 1) were carried out to evaluate the performance of FTVI systems using various working fluids under different operating conditions. The studies unanimously found that the system capacity and COP improved when vapor injection was applied. In low ambient temperature heating applications, heating capacity and COP could increase by 45% and 24%, respectively, compared to non-injection systems (Baek et al., 2008). In high ambient temperature cooling applications, cooling capacity and COP improved by 14.2% and 16.5%, respectively (Cho et al., 2009).

Despite all the advantages, FTVI systems are more difficult to control compared to the conventional systems. Instead, a proper liquid level in the flash tank needs to be maintained during the operation (Xu et al., 2011a). Moreover, the same authors (Xu et al., 2011b) experimentally demonstrated that the superheat of the injected vapor could be used as the control signal to the upper-stage expansion valve. In order to maintain sufficient superheat of the injected vapor, an electric heater with constant power input was applied on the injection line.

The purpose of the present paper differs from the study by Xu et al. (2011b) by focusing on the numerical modeling, to investigate the controllability of FTVI systems, and to gain the knowledge about the liquid level fluctuation during cycling operation, which might help in optimizing the size of the flash tank.

Transient modeling of vapor compression systems dates back to 1970s (Winkler, 2009). Comprehensive review of the literature (Bendapudi and Braun, 2002; Rasmussen, 2012) in this field indicates that a majority of the previous studies focused on conventional, single-stage vapor compression systems, and no studies have focused on FTVI systems. Therefore, this two-part article attempts to broaden this aspect of research and explore the dynamic behavior of such systems. The first part introduces a first-principles model that describes the heat transfer and flow phenomena of FTVI systems under transient conditions. The second part presents the cycling transients of the system and a detailed comparison between simulation results and experimental data.

2. System description

The studied system and its log(p)-h diagram are shown in Fig. 1. The high pressure and high temperature vapor (2) discharged by the compressor enters the condenser. The refrigerant passing through the condenser rejects heat to the high temperature reservoir and changes to a subcooled liquid (3).

Table 1 – FTVI experimental studies.

Citation	Refrigerant	Application	Operating conditions			
			Indoor		Outdoor	
			DB (°C)	WB (°C)	DB (°C)	WB (°C)
Baek et al. (2008)	CO_2	Heating	20	15	7	6
Cho et al. (2009)	CO_2	Cooling	27	19.5	35	24
Wang et al. (2009)	R410A	Cooling	27.8		26.7	19.4
			35			
			46.1			
		Heating	16.7	14.7	21.1	≤ 15.6
			8.3	6.1		
			−8.3	−9.4		
			−17.8			
Xu et al. (2013b)	R410A & R32	Cooling	27.8		26.7	19.4
			35			
			46.1			
		Heating	8.3	6.1	21.1	
			−8.3	−9.4		
			−17.8			
			Condensing Temperature (°C)		Evaporating Temperature (°C)	
Ma and Zhao (2008)	R22	heating	42 & 45		−25 to −7	
Xu et al. (2013a)	R32	cooling	40 & 45		5	
		heating	40 & 45		−10, −5 & 0	

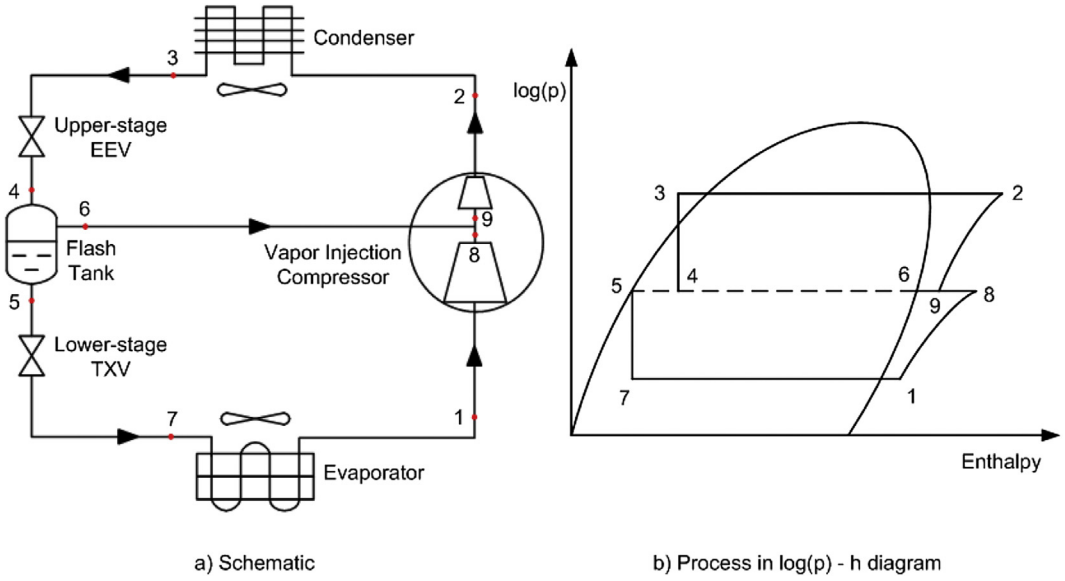

Fig. 1 – FTVI system: a) Schematic; b) Process in log(p) – h diagram.

Then, the refrigerant flows through the upper-stage expansion valve and undergoes a drastic drop in pressure. This process results in a vapor–liquid mixture that enters the flash tank (4) where the vapor and liquid separate. The saturated vapor (6) is injected to the compressor. The saturated liquid (5) flows through the lower-stage expansion valve and undergoes another throttling process. The low pressure, low temperature, and low quality refrigerant (7) enters the evaporator, where it gains heat from the low temperature reservoir and reaches a superheated vapor state (1) at the evaporator exit. The compressor receives the refrigerant at state (1) and compresses it to an intermediate pressure (8) during the first compression stage, after which the refrigerant mixes with the injected vapor. Finally, the mixed refrigerant (9) is further compressed to a high pressure during the second compression stage. The compression process is associated with an increase in refrigerant temperature.

3. Mathematical modeling

3.1. *Compressor model*

A vapor injection scroll compressor was used in this experiment. Fig. 2 displays various elements of a vapor injection scroll compressor and the refrigerant flow path. Vapor injection can be turned on or off by opening or closing the solenoid valve prior to the economizer port on the injection line. In the present study, the solenoid valve is kept open to enable vapor injection. Refrigerant leaving the evaporator enters the suction chamber. This refrigerant absorbs heat from the metallic elements, and cools the motor before being drawn into the compression chamber. At the transition point of the compression process, the refrigerant compressed to the intermediate pressure mixes with the injected vapor from the economizer port and completes the remaining compression process before being discharged into the discharge chamber.

The compressor is divided into separate lumps with internal heat transfer (Fig. 3) and analyzed with the following assumptions:

(1) there is no pressure drop inside the suction chamber;
(2) the oil effects are negligible;
(3) any refrigerant entering the suction chamber mixes homogeneously with the refrigerant inside the suction chamber before being drawn into the scrolls;
(4) heat conduction and radiation between metallic elements are neglected;
(5) the compression process is presumably completed in one large pocket;
(6) the low and high stage compression processes are assumed to have the same polytropic index.

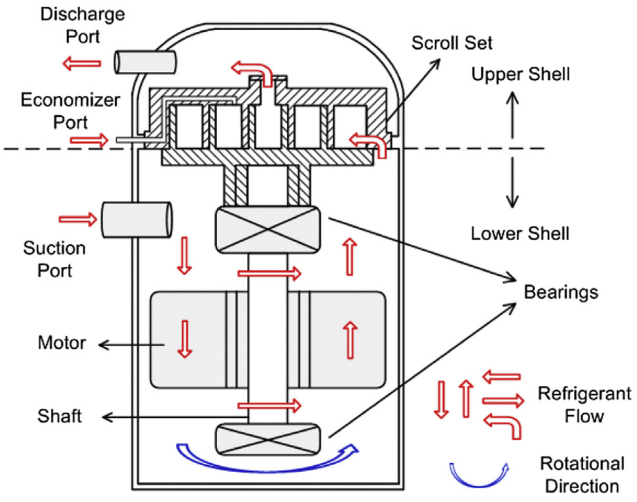

Fig. 2 – Schematic of a vapor injection scroll compressor.

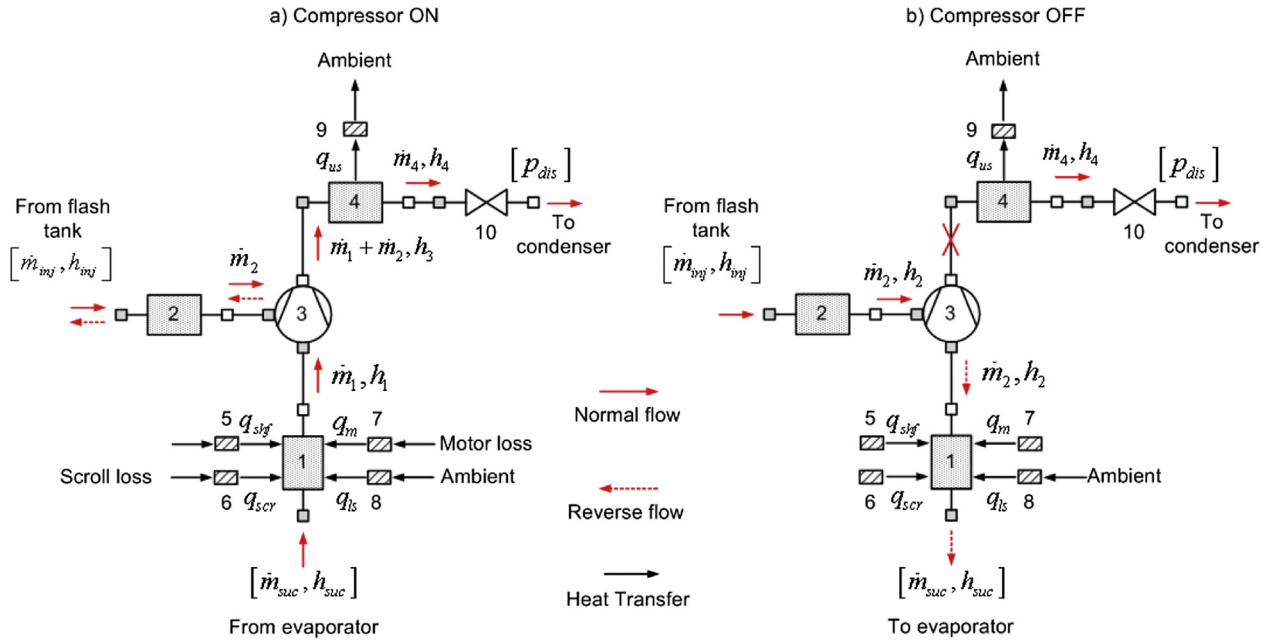

Fig. 3 – Model representation of a vapor injection scroll compressor: 1 – suction chamber control volume; 2 – economizer port control volume; 3 – compression process; 4 – discharge chamber control volume; 5 – shaft and bearings; 6 – scroll set; 7 – motor; 8 – low-side shell; 9 – high-side shell; 10 – discharge port pressure loss.

The boundary conditions of the compressor model are defined as the mass flow rate and enthalpy entering the suction port, the mass flow rate and enthalpy entering the economizer port, and the discharge pressure. As a result, a small control volume at the economizer port and a discharge pressure loss are included in the model. The reason of such boundary conditions will be explained in Section 4.1.

3.1.1. *Compressor on*

The mass and energy conservation of the refrigerant within the suction chamber (CV 1) can be described as.

$$V_1\frac{d\rho_1}{dt} = \dot{m}_{suc} - \dot{m}_1 \tag{1}$$

$$V_1\left(\rho_1\frac{dh_1}{dt} - \frac{dp_1}{dt}\right) = \dot{m}_{suc}(h_{suc} - h_1) + q_{ls} + q_m + q_{shf} + q_{scr} \tag{2}$$

Similarly, the mass and energy conservation equations for the refrigerant in the discharge chamber can be formulated.

The heat transfer between the refrigerant and pertinent elements is determined as follows:

$$\begin{cases} q_{ls} = \dfrac{T_{ls} - T_1}{R_{rls}} \\ q_m = \dfrac{T_m - T_1}{R_{rm}} \\ q_{shf} = \dfrac{T_{shf} - T_1}{R_{rshf}} \\ q_{scr} = \dfrac{T_{scr} - T_1}{R_{rscr}} \end{cases} \tag{3}$$

The refrigerant in the suction chamber is not necessarily superheated, and the compressor might experience liquid flooding at the very beginning of the start-up operation. Therefore, adopting constant thermal resistances might not be appropriate in the simulation. In order to estimate the thermal resistances accurately, the heat transfer area of each metallic element is measured, and the corresponding heat transfer coefficients are calculated using empirical correlations according to the refrigerant state in the suction chamber. Specifically, the Dittus-Boelter (1985) correlation and the Gungor-Winterton (1987) correlation are used for single-phase and two-phase heat transfer coefficient calculations, respectively. During the "off-period", the Churchill-Chu (1975) correlation and the Cooper (1984) correlation are used to calculate the natural convection and boiling heat transfer coefficient, respectively.

The motor efficiency and mechanical efficiency are defined as.

$$\eta_m = \frac{\dot{W}_{shf}}{\dot{W}_{tot}} \tag{4}$$

$$\eta_{mech} = \frac{\dot{W}_{comp}}{\dot{W}_{shf}} \tag{5}$$

The thermal storage for various metallic elements of the compressor can be formulated as.

$$M_{ls}c_{p,ls}\frac{dT_{ls}}{dt} = \frac{T_{amb} - T_{ls}}{R_{als}} - q_{ls} \tag{6}$$

$$M_{us}c_{p,us}\frac{dT_{us}}{dt} = \frac{T_{amb} - T_{us}}{R_{aus}} - q_{us} \tag{7}$$

$$M_m c_{p,m}\frac{dT_m}{dt} = (1 - \eta_m)\dot{W}_{tot} - q_m \tag{8}$$

$$M_{shf}c_{p,shf}\frac{dT_{shf}}{dt} = \xi_{shf}(1-\eta_{mech})\dot{W}_{shf} - q_{shf} \tag{9}$$

$$M_{scr}c_{p,scr}\frac{dT_{scr}}{dt} = (1-\xi_{shf})(1-\eta_{mech})\dot{W}_{shf} - q_{scr} \tag{10}$$

The refrigerant mass flow rate drawn by the scroll set from CV 1 is calculated as.

$$\dot{m}_1 = \left[a_1 - a_2\left(\frac{p_4}{p_1}\right)^{\frac{1}{n}}\right]\rho_1 V_{disp}\frac{N}{60} \tag{11}$$

where the polytropic index n is estimated to be 1.35 based on the compressor performance test.

The injection flow is calculated by conceiving the injection port as a fixed orifice through which the reverse flow can possibly occur.

$$\dot{m}_2 = \mathrm{sign}(p_2 - p_{\mathrm{int}})\cdot a_3\sqrt{\rho_{\mathrm{in}}|p_2 - p_{\mathrm{int}}|} \tag{12}$$

where p_{int} is the internal intermediate pressure after the first stage compression (state point 8 in Fig. 1) and can be determined by assuming a polytropic compression process

$$\frac{p_{\mathrm{int}}}{p_1} = \zeta^n \tag{13}$$

where the built-in volume ratio of the first stage ζ is 1.21 in the present study.

The flow direction through the economizer port is dependent on the difference between the pressure at the economizer port control volume and the internal intermediate pressure. If the pressure difference is positive, the compressor will absorb the vapor from the flash tank. If the pressure difference is negative, the compressed vapor after the first stage compression will be discharged to the flash tank, as observed at the very beginning of the start-up operation.

As a consequence, the conservation of mass and energy for the control volume at the economizer port (CV 2) should be considered separately for these two scenarios assuming negligible heat transfer.

$$V_2\frac{d\rho_2}{dt} = \dot{m}_{inj} - \dot{m}_2 \tag{14}$$

$$V_2\left(\rho_2\frac{dh_2}{dt} - \frac{dp_2}{dt}\right) = \begin{cases} \dot{m}_{inj}(h_{inj} - h_2) & \text{when } p_2 - p_{\mathrm{int}} \geq 0 \\ -\dot{m}_2(h_{\mathrm{int}} - h_2) & \text{when } p_2 - p_{\mathrm{int}} < 0 \end{cases} \tag{15}$$

where $\dot{m}_{inj}$ and $\dot{m}_2$ are positive for the normal flow and negative for the reverse flow. The refrigerant temperature after the first stage compression can be calculated as

$$T_{\mathrm{int}} = T_1\left(\frac{p_{\mathrm{int}}}{p_1}\right)^{\frac{n}{n-1}} \tag{16}$$

Refrigerant enthalpy after mixing (point 9, Fig. 1) the suction flow and injection flow can be determined through the energy conservation.

$$h_{mix} = \begin{cases} \dfrac{\dot{m}_1 h_{\mathrm{int}} + \dot{m}_2 h_2}{\dot{m}_1 + \dot{m}_2} & \text{when } p_2 - p_{\mathrm{int}} > 0 \\ h_{\mathrm{int}} & \text{when } p_2 - p_{\mathrm{int}} \leq 0 \end{cases} \tag{17}$$

The polytropic compression work is evaluated as.

$$\dot{W}_{comp} = \frac{n}{n-1}\left\{p_1\dot{V}_1\left[\left(\frac{p_{\mathrm{int}}}{p_1}\right)^{\frac{n}{n-1}} - 1\right] + p_{\mathrm{int}}\dot{V}_{mix}\left[\left(\frac{p_4}{p_{\mathrm{int}}}\right)^{\frac{n}{n-1}} - 1\right]\right\} \tag{18}$$

where $\dot{V}_1$ and $\dot{V}_{mix}$ are the volumetric flow rates evaluated based on ρ_1 and ρ_{mix}, respectively.

The refrigerant temperature after the entire compression process is.

$$T_3 = T_{mix}\left(\frac{p_4}{p_{\mathrm{int}}}\right)^{\frac{n-1}{n}} \tag{19}$$

The discharge mass flow rate is determined through the following expression.

$$\dot{m}_4 = \frac{\sqrt{\rho_4(p_4 - p_{dis})}}{f_{dis}} \tag{20}$$

Finally, the total power input required by the compressor is determined via the following correlation deduced from the compressor performance map.

$$\dot{W}_{tot} = b_1 p_1\dot{V}_1\left[\left(\frac{p_{\mathrm{int}}}{p_1}\right)^{b_2} - 1\right] + b_3 p_{\mathrm{int}}\dot{V}_{mix}\left[\left(\frac{p_4}{p_{\mathrm{int}}}\right)^{b_4} - 1\right] + b_5 \tag{21}$$

3.1.2. *Compressor off*

During the "off-period", the compressor stops pumping the refrigerant to the discharge side, which is disconnected from the suction side to prevent backflow by the internal check valve. However, the flash tank is still connected to the low-pressure suction side by the economizer port. As a result, refrigerant from the injection line will travel through the economizer port to the suction chamber (Fig. 3b). In this case, the mass flow rate through the economizer port is.

$$\dot{m}_2 = a_3\sqrt{\rho_2(p_2 - p_1)} \tag{22}$$

The suction chamber is modeled as an accumulator with internal heat transfer and the governing equations are.

$$V_1\frac{d\rho_1}{dt} = \dot{m}_{suc} + \dot{m}_2 \tag{23}$$

$$V_1\left(\rho_1\frac{dh_1}{dt} - \frac{dp_1}{dt}\right) = \dot{m}_2(h_2 - h_1) + \dot{m}_{suc}(h_{suc} - h_1) + q_{ls} + q_m + q_{shf} + q_{scr} \tag{24}$$

where $\dot{m}_{suc}$ is negative, denoting that the refrigerant is flowing out of the control volume. h_{suc} is the enthalpy of the refrigerant leaving the suction chamber, which is determined by the state of the refrigerant inside the suction chamber. For modeling details, readers should refer to Section 3.4 for the flash tank modeling, since the only difference is that the accumulator only has the vapor outlet. Other parts of the compressor can be analyzed by applying the same equations for the "on-period" by recognizing that the power consumption is zero for the "off-period".

The selection of state variables has a decisive effect on the simulation speed. In this study, unless specified otherwise, the pressure p and the enthalpy h have been selected as the state variables because they usually serve as the independent properties of property routines. Moreover, the enthalpy can

also act as the independent state variable to distinguish whether the refrigerant is single-phase or two-phase, and therefore appropriate correlations for heat transfer and pressure drop can be applied accordingly. As a result, the derivative of the density with respect to the time in the continuity equation can be expanded as follows.

$$\frac{d\rho}{dt} = \frac{\partial\rho}{\partial p}\bigg|_h \frac{dp}{dt} + \frac{\partial\rho}{\partial h}\bigg|_p \frac{dh}{dt} \tag{25}$$

The partial derivatives of the density can be calculated either analytically based on the thermodynamic relations or numerically.

3.2. Expansion device models

In the system, an electronic expansion valve (EEV) is used in the upper-stage and a thermostatic expansion valve (TXV) is used in the lower-stage. The following assumptions are made:

(1) the valve is adiabatic;
(2) the expansion process is isenthalpic;
(3) TXV bulb content is at the uniform temperature;
(4) the friction and inertia of the mechanical parts are negligible.

3.2.1. Electronic expansion valve

In general, injection flow is either a saturated vapor or in two-phase. An electric heater with 60 W power input was attached to the surface of the injection line in order to maintain injection superheat. A pressure sensor and an in-stream thermocouple were installed in the injection line to measure the pressure and temperature of the injected vapor, respectively. As such, the superheat of the injected vapor can be determined. The injection superheat signal is received by the EEV controller, which adjusts the opening of the valve.

The mass flow rate through the throttle is determined by the flow coefficient, the flow area, the inlet density, and the pressure difference across the valve.

$$\dot{m}_{\text{exp}} = C_v A\sqrt{\rho_{\text{in}}\Delta p} \tag{26}$$

The combined value of the product C_vA can be readily obtained by regression based on the experimental data.

$$C_vA = c_0 + c_1\varphi + c_2\varphi^2 + c_3\varphi^3 \tag{27}$$

where $\varphi$is the percentage of valve opening determined by the PID controller based on error between the measured superheat and the set point, $e_{\text{sh}}(t)$

$$\varphi(t) = K_p e_{sh}(t) + K_i\int_0^t e_{sh}(\tau)d\tau + K_d\frac{d}{dt}e_{sh}(t) \tag{28}$$

3.2.2. Thermostatic expansion valve

The TXV comprises of two portions: the throttling portion and the sensor bulb portion. The throttling portion regulates the refrigerant mass flow through the valve, and the sensor bulb portion monitors the refrigerant temperature leaving the evaporator. The sensor bulb also converts the change in temperature into the change in pressure on the diaphragm, causing the needle to move upwards or downwards.

The sensor bulb is modeled as a lumped section and the relationship between the bulb temperature and the refrigerant temperature at the evaporator outlet is given by.

$$\tau_b\frac{dT_b}{dt} = T_{r,eo} - T_b \tag{29}$$

The spring deflection needs to be determined in order to find the effective flow area. The force exerted by the spring can be found from a force balance on the diaphragm (Fig. 4a). The spring force is assumed to be a linear function of the spring deflection, yielding.

$$\kappa y + F_{offset} = \left(p_b - p_{eq}\right)A_{diaph} \tag{30}$$

where F_{offset} is the initial spring force.

The effective flow area, defined as the minimum free flow area that the refrigerant passes through the valve, can be calculated based on the valve geometry (Fig. 4b, c and 4d).

$$A = \min\left[\pi\left(d_{ori} - \frac{y}{2}\sin 2\beta\right)y\cos\beta, \frac{\pi}{4}\left(d_{ori}^2 - d_{pin}^2\right)\right] \tag{31}$$

Equation (26) is used to determine the mass flow rate through the throttle. When the valve is fully open, the maximum flow rate corresponding to the actual conditions is reached. Manufacturers predict that the maximum flow rate can be between 110% and 140% of the rated flow rate (ASHRAE, 1998). The flow coefficient can be determined by assuming that the valve is fully open when the maximum mass flow rate is 20% greater than the value of nominal operating conditions (Fu et al., 2003), i.e.

$$C_v = \frac{1}{A_{\max}}\left(\frac{1.2\dot{m}}{\sqrt{\rho\Delta p}}\right)_{rated} \tag{32}$$

3.3. Heat exchanger model

A segment-by-segment heat exchanger model is employed. Each heat exchanger segment is divided into three sections, i.e. the refrigerant flow, finned walls, and air stream.

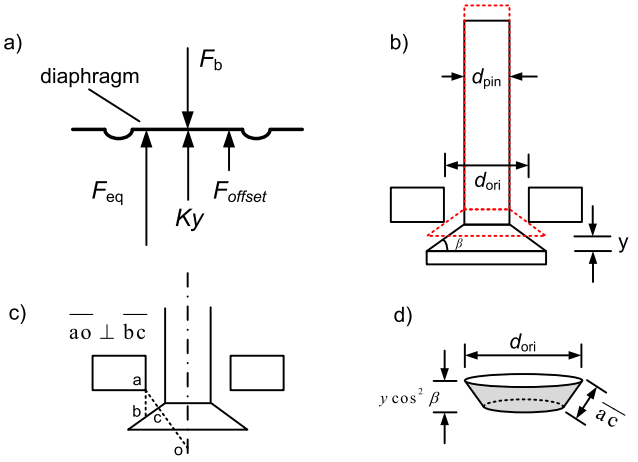

Fig. 4 – a) Force balance on the diaphragm; b) Valve geometry; c) Various lengths; d) Effective flow area.

3.3.1. *Refrigerant flow*

The refrigerant flow is simplified as a one-dimensional flow with fluid properties varying only in the direction of flow. In other words, fluid properties are uniform or averaged at every cross section along the axis of the channel. Additionally, the following assumptions are made.

1) the fluid is Newtonian;
2) the axial heat conduction in the refrigerant flow direction is ignored;
3) negligible viscous dissipation;
4) in the two-phase region, the liquid and vapor are in thermodynamic equilibrium;
5) the potential energy and kinetic energy of the refrigerant are neglected;
6) dynamic pressure waves are of minor importance and thus neglected in the momentum equation (Brasz and Koenig, 1983).

Thus, the conservation laws can be formulated as follows (Levy, 1999)

$$\frac{\partial}{\partial t}(\overline{\rho}A)+\frac{\partial}{\partial z}(GA)=0 \tag{33}$$

$$\frac{\partial}{\partial t}\left(\overline{\rho}\overline{h}_{\rho}A\right)+\frac{\partial}{\partial z}\left(G\overline{h}A\right)=Pq''_{w}+\frac{\partial}{\partial t}(pA) \tag{34}$$

$$A\frac{\partial p}{\partial z}+\overline{\tau}_{w}P=0 \tag{35}$$

where

$$\overline{\rho}=\frac{1}{A}\int_{A}\rho dA=\text{average density at z} \tag{36}$$

$$G=\frac{1}{A}\int_{A}\rho u dA=\text{average mass flow per unit area at z} \tag{37}$$

$$\overline{h}_{\rho}=\frac{1}{\overline{\rho}}\left(\frac{1}{A}\int_{A}\rho h dA\right)=\text{average density}-\text{weighted enthalpy at z} \tag{38}$$

$$\overline{h}=\frac{1}{G}\left(\frac{1}{A}\int_{A}\rho u h dA\right)=\text{average flow}-\text{weighted enthalpy at z} \tag{39}$$

$$\overline{\tau}_{w}=\frac{1}{P}\int_{P}\tau_{w}dl=\text{average wall shear stress at z} \tag{40}$$

$$q''=\text{average surface heat flux} \tag{41}$$

For the single-phase flow, the refrigerant density can be presumed uniform at the cross sectional area, and the following relations can be readily obtained.

$$\overline{\rho}=\rho \tag{42}$$

$$\overline{h}_{\rho}=\overline{h}=h \tag{43}$$

For the two-phase flow, average density and enthalpies are determined by.

$$\overline{\rho}=\rho_{g}\gamma+\rho_{f}(1-\gamma) \tag{44}$$

$$\overline{h}_{\rho}=\frac{1}{\overline{\rho}}\left[\rho_{g}h_{g}\gamma+\rho_{f}h_{f}(1-\gamma)\right] \tag{45}$$

$$\overline{h}=\frac{1}{G}\left[\rho_{g}u_{g}h_{g}\gamma+\rho_{f}u_{f}h_{f}(1-\gamma)\right]=h_{g}x+h_{f}(1-x) \tag{46}$$

where the void fraction and flow quality are defined as follows

$$\gamma=\frac{\text{area of gas}}{\text{total area}}=\frac{A_{g}}{A_{g}+A_{f}}=\frac{A_{g}}{A} \tag{47}$$

$$x=\frac{\text{mass flow of gas}}{\text{total mass flow}}=\frac{\rho_{g}u_{g}\gamma}{\rho_{g}u_{g}\gamma+\rho_{f}u_{f}(1-\gamma)}=\frac{\rho_{g}u_{g}\gamma}{G} \tag{48}$$

It is understandable to confuse the flow quality x with the static quality $\hat{x}$, which is defined as the ratio of mass of vapor to that of mixture.

$$\hat{x}=\frac{M_{g}}{M_{g}+M_{f}}=\frac{\rho_{g}\gamma}{\rho_{g}\gamma+\rho_{f}(1-\gamma)} \tag{49}$$

Hence, the density-weighted enthalpy can be denoted by the static quality.

$$\overline{h}_{\rho}=\hat{x}h_{g}+(1-\hat{x})h_{f} \tag{50}$$

In the analysis of two-phase flows, the assumption of a homogeneous flow is often adopted when the liquid and vapor phases are in thermodynamic equilibrium, and have the same phase velocity. However, this assumption is inappropriate in some cases, e.g. a large portion of the evaporator is annular flow. Moreover, this assumption results in a prediction of lower refrigerant mass and rapid transients (Kærn et al., 2011). Quite a few publications (MacArthur and Grald, 1989; Plough-Sørensen et al., 1997; Mithraratne et al., 2000; Koury et al., 2001; Haberschill et al., 2003; Ndiaye and Bernier, 2010; Choi et al., 2011) tried to account for the slip effect of two-phase flows by using the homogeneous flow model corrected by void fraction model. Unfortunately, these studies were unable to distinguish the density-weighted enthalpy $\overline{h}_{\rho}$ from the flow-weighted enthalpy $\overline{h}$ in the energy equation, and used the flow-weighted enthalpy $\overline{h}$ instead in place of the density-weighted enthalpy $\overline{h}_{\rho}$. Although this results in a significant simplification for the computation, it is fundamentally erroneous because these two enthalpies are only equivalent to each other under the assumption of homogeneous flow.

In the present analysis, separated flow model (SFM) without interfacial exchange is used. SFM allows only velocity to differ for the two phases. Thus the original form of conservation equations for homogeneous flow can be preserved with few modifications by introducing variables for mixtures.

Bauer (1999) proposed a method to correct the mass flow rate to account for the difference in phasic velocities since the transient form of momentum equation was used in his model. In his model, the two-phase slip-ratio needs to be calculated explicitly, which is sometimes impossible for non-slip-ratio-based void fraction models. In light of this, the presented paper intends to introduce a more generalized and

Table 2 – Constants and exponents for various void fraction models.

Models	c	q	r	s
Homogeneous	1	1	1	0
Zivi (1964)	1	1	0.67	0
Turner (1966)	1	0.72	0.40	0.08
Smith (1969)	0.79	0.78	0.58	0
Lockhart-Martinelli (1949)	0.28	0.64	0.36	0.07
Thome (1964)	1	1	0.89	0.18
Baroczy (1965)	1	0.74	0.65	0.13

straightforward approach to calculate the flow-weighted enthalpy based on its definition, which is the essence of SFM.

The analysis first selects the pressure p and the density-weighted enthalpy $\overline{h}_\rho$ as the state variables (the partial derivatives of the density are still required, see Equation (25)). Since $\overline{h}_\rho$ is the state variable, it is known at each time step. If an expression can be established that relates $\overline{h}_\rho$ and $\overline{h}$, the computation will become much more tractable.

This introduces the enthalpy correction Δh_c

$$\begin{aligned}\Delta h_c &= \overline{h} - \overline{h}_\rho \\ &= xh_g + (1-x)h_f - \hat{x}h_g - (1-\hat{x})h_f \\ &= (x-\hat{x})(h_g - h_f)\end{aligned} \tag{51}$$

It should be noted here that x and $\hat{x}$ are zero for the subcooled liquid, and unity for the superheated vapor, respectively. Hence, Δh_c becomes zero for single-phase flows.

All the variables in Equation (51) are the thermodynamic properties, and can be readily calculated except for the flow quality x. Specifically, h_g and h_f can be evaluated based on the pressure, whereas the static quality $\hat{x}$ can be obtained via Equation (50) since $\overline{h}_\rho$ is known at every time step.

Butterworth (1975) has shown that the slip-ratio-based void fraction equations can be fit to a standard expression form of

$$x = \frac{\gamma^{1/q}}{\gamma^{1/q} + \left[\frac{1}{c}\left(\frac{\rho_f}{\rho_g}\right)^r \left(\frac{\mu_g}{\mu_f}\right)^s\right]^{1/q} (1-\gamma)^{1/q}} \tag{52}$$

The constants and exponents for different void fraction models are given in Table 2.

The procedure of calculating the flow-weighted enthalpy $\overline{h}$ is given in Fig. 5. By using the enthalpy correction method described above, the same set of governing equations 33–35 can be applied to both single-phase and two-phase flows without requiring any modifications. Meanwhile, Equation (51) ensures that the correction only applies for the two-phase flow and gives a seamless transition between the single-phase and two-phase flows. Furthermore, by selecting p and $\overline{h}_\rho$ as the state variables, all the thermophysical properties, including the partial derivatives of the density, can be calculated in a consistent manner irrespective of the type of void fraction model used.

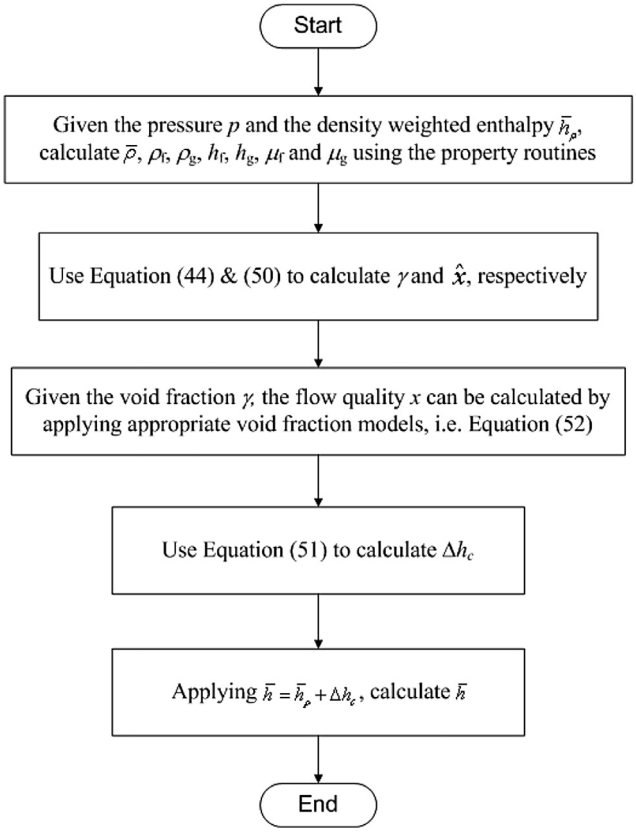

Fig. 5 – Flowchart for calculating the flow-weighted enthalpy.

3.3.2. *Air side*

The air side (Fig. 6) is analyzed based on the following assumptions.

1) one-dimensional quasi-steady airflows;
2) negligible conduction in air flow direction;
3) the temperature profile within fins follows the steady-state profile, allowing the use of heat transfer and combined heat and mass transfer fin efficiencies;
4) simultaneous heat and mass transfer follows the Lewis analogy;
5) equal temperature of tube wall and fins at one section.

3.3.2.1. *Fan on.* The governing equations for the air side are

$$\dot{m}_a c_{p,a} \frac{dT_a}{dy}\Delta y = \alpha_a \left(A_{o,t} + \eta_{fin} A_{o,fin}\right)(T_w - T_a) \tag{53}$$

$$\dot{m}_a \frac{d\omega_a}{dy}\Delta y = \alpha_m \left(A_{o,t} + \eta_{fin} A_{o,fin}\right)\min(0, \omega_{w,sat} - \omega_a) \tag{54}$$

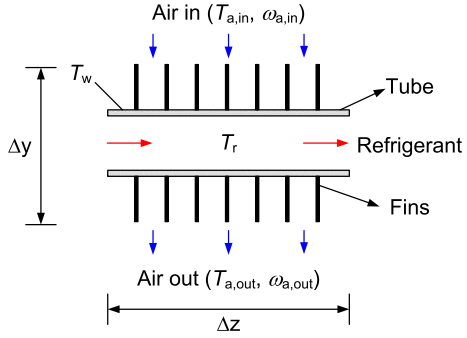

Fig. 6 – A discretized heat exchanger segment.

where $\omega_{w,sat}$ is the humidity ratio of saturated air evaluated at T_w and the fin efficiency is calculated using the equation proposed by Hong and Webb (1996). The mass transfer coefficient α_m is determined by applying the Lewis analogy

$$\alpha_m = \frac{\alpha_a}{c_{p,a} Le^{2/3}} \tag{55}$$

where $Le^{2/3} = 0.9$ (Kuehn et al., 1998).

3.3.2.2. *Fan off*. When the fan is off, the heat exchange between the ambient air and the heat exchanger is dominated by natural convection. In this case, the heat transfer is calculated by neglecting dehumidification and assuming the air temperature is uniform for the entire heat exchanger.

Radiation heat transfer needs to be taken into account for the outer most tubes, i.e. the tubes in the first and last tube bank, which are directly exposed to the ambient. For each segment of these tubes, one can have

$$q_a = \alpha_a \left(A_{o,t} + \eta_{fin} A_{o,fin}\right)(T_a - T_w) + \varepsilon\sigma A_{face}\left(T_a^4 - T_w^4\right) \tag{56}$$

where A_{face} is the frontal area and ε is the emissivity of fin material (0.04 for aluminum foil), respectively.

3.3.3. *Tube walls and fins*

Without considering the axial conduction along the tube, the energy equation of the tube walls and associated fins is

$$\left(M_t c_{p,t} + M_{fin} c_{p,fin}\right)\frac{dT_w}{dt} = q_r + q_a \tag{57}$$

where

$$q_r = \alpha_r A (T_r - T_w) \tag{58}$$

$$q_a = \dot{m}_a \left[c_{p,a}\left(T_{a,in} - T_{a,out}\right) + \left(\omega_{a,in} - \omega_{a,out}\right)\Delta h_{fg}\right] \tag{59}$$

3.4. *Flash tank model*

The liquid–vapor refrigerant mixture enters the flash tank, separates, and exits as single-phase (Fig. 7). The flash tank is modeled as a lumped control volume with one inlet and two outlets by adopting the following simplifications:

(1) ideal phase separation;
(2) vapor and liquid in the flash tank are in thermodynamic equilibrium;
(3) pressure drop inside the flash tank is negligible;
(4) adiabatic flash tank.

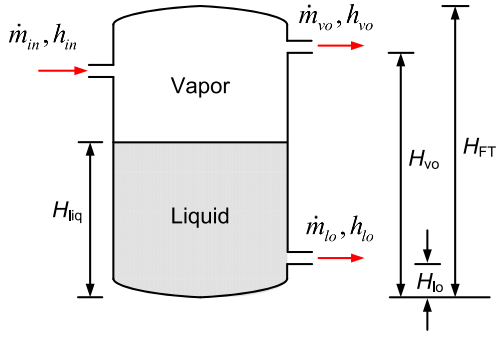

Fig. 7 – Schematic of the flash tank.

The governing equations for the flash tank can be described as follows

$$V_{FT}\frac{d\overline{\rho}_{FT}}{dt} = \dot{m}_{in} - \dot{m}_{lo} - \dot{m}_{vo} \tag{60}$$

$$V_{FT}\left(\overline{\rho}_{FT}\frac{d\overline{h}_{FT}}{dt} - \frac{dp_{FT}}{dt}\right) = \dot{m}_{in}\left(h_{in} - \overline{h}_{FT}\right) - \dot{m}_{lo}\left(h_{lo} - \overline{h}_{FT}\right) - \dot{m}_{vo}\left(h_{vo} - \overline{h}_{FT}\right) \tag{61}$$

The leaving enthalpies of the vapor and liquid streams are dependent on the state of the refrigerant in the flash tank. There are two cases that need to be taken into account: 1) the refrigerant state is two-phase $(h_f < \overline{h}_{FT} < h_g)$ and 2) the refrigerant state is single-phase $(\overline{h}_{FT} <= h_f \quad \text{or} \quad \overline{h}_{FT} >= h_g)$.

Case 1. *Leaving enthalpies of two outlet streams are determined as*

$$h_{lo} = \begin{cases} h_f & \text{if } H_{liq} > H_{lo} + d_{liq} \\ h_g - \left(\dfrac{H_{liq} - H_{lo}}{d_{liq}}\right)(h_g - h_f) & \text{if } H_{lo} + d_{liq} \geq H_{liq} \geq H_{lo} \\ h_g & \text{if } H_{liq} < H_{lo} \end{cases}$$

$$h_{vo} = \begin{cases} h_f & \text{if } H_{liq} > H_{vo} + d_{vap} \\ h_g - \left(\dfrac{H_{liq} - H_{vo}}{d_{vap}}\right)(h_g - h_f) & \text{if } H_{vo} + d_{vap} \geq H_{liq} \geq H_{vo} \\ h_g & \text{if } H_{liq} < H_{vo} \end{cases} \tag{62}$$

where the liquid height is determined as

$$H_{liq} = \frac{\overline{\rho}_{FT} - \rho_g}{\rho_f - \rho_g} H_{FT} \tag{63}$$

Case 2. *Leaving enthalpies of the two outlet streams should be equal to the mean enthalpy of the refrigerant in the flash tank*

$$\begin{cases} h_{lo} = \overline{h}_{FT} \\ h_{vo} = \overline{h}_{FT} \end{cases} \tag{64}$$

The mass flow rate of the two steams can be calculated by

$$\begin{cases} \dot{m}_{lo} = \dfrac{\sqrt{\rho_f\left(p_{FT} - p_{lo}\right)}}{f_{liq}} \\ \dot{m}_{vo} = \dfrac{\sqrt{\rho_g\left(p_{FT} - p_{vo}\right)}}{f_{vap}} \end{cases} \tag{65}$$

3.5. *Reversing valve model*

The reversing valve is used to switch between cooling and heating in a heat pump system by changing the refrigerant flow direction. In this study, the reversing valve is represented by two control volumes and two pairs of throttles (Fig. 8). Only one pair of throttles is kept at a full operational position at a time, denoting the on-state, whereas the other pair is operating in a minimum opening position, denoting the off-state. Heat exchange between the hot stream and cold stream is

accounted for. The leakage through the pair of closed throttles is also considered.

The conservation of mass and energy for the high-side and low-side control volumes can be analyzed without difficulty by following the analysis for the compressor, and will not be presented here.

The on/off state of the throttles is not changed instantaneously during the transition between cooling and heating mode, the opening of the throttle is assumed to follow the expression below

$$\frac{d\varphi}{dt} = \frac{1}{\tau}\left(\varphi_{\text{target}} - \varphi\right) \tag{66}$$

where φ_{target} is the target opening, 100% for the on-state and 0.01% for the off-state.

The mass flow rate through the throttles can be calculated by taking the form of Equation (20) with the appropriate density and pressure difference, and finally it needs to be multiplied by the current opening, i.e.

$$\dot{m} = \varphi\frac{\sqrt{\rho_{in}\Delta p}}{f} \tag{67}$$

The heat transfer between the hot stream and cold stream is evaluated based on the thermal resistance, i.e.

$$q_{rev} = \frac{T_{hs} - T_{cs}}{R_{hcs}} \tag{68}$$

where R_{hcs} is estimated to be 1.0 K/W based on the measured refrigerant temperature difference across the suction side of the valve under the steady-state operation.

With the proposed reversing valve model, the same integral system model can be utilized to simulate both cooling and heating mode, therefore two separate models are no longer required. This is particularly convenient to model system transients during a reverse cycle defrosting. The proposed model structure allows all the component models to be linked systematically so that two control volumes are not directly coupled without an intermediate throttle during the transition stages between cooling and heating mode.

There are also two three-way valves before the flash tank in the experimental setup to change the refrigerant flow direction, ensuring that the inlet and outlet are not switched in the reversed mode. The reversing valve model, without applying heat exchange, is used to simulate this dual three-way valve configuration in the study.

3.6. *Pipe model*

A large portion of refrigerant resides in the connecting pipes, contributing significantly to the transient characteristics of the system. The governing equations for the pipe model are essentially the same as those for the heat exchanger model, except that the air side heat transfer is natural convection. Readers are referred to Section 3.3 for the heat exchanger modeling.

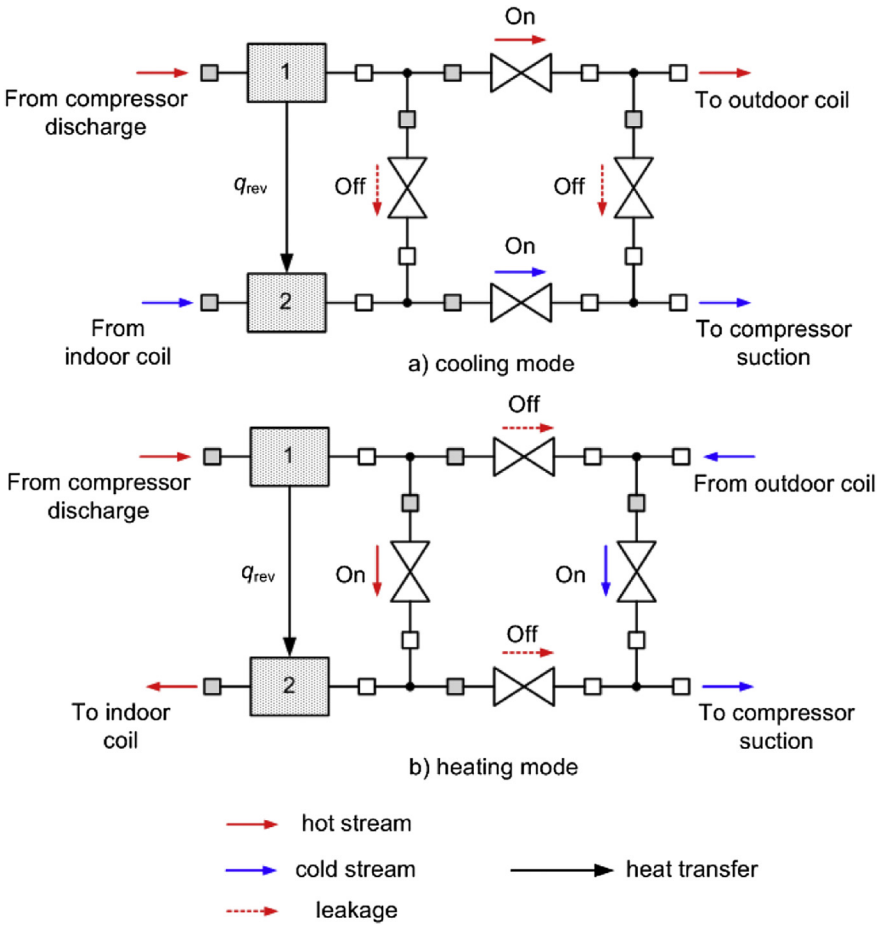

Fig. 8 – Model representation of a reversing valve.

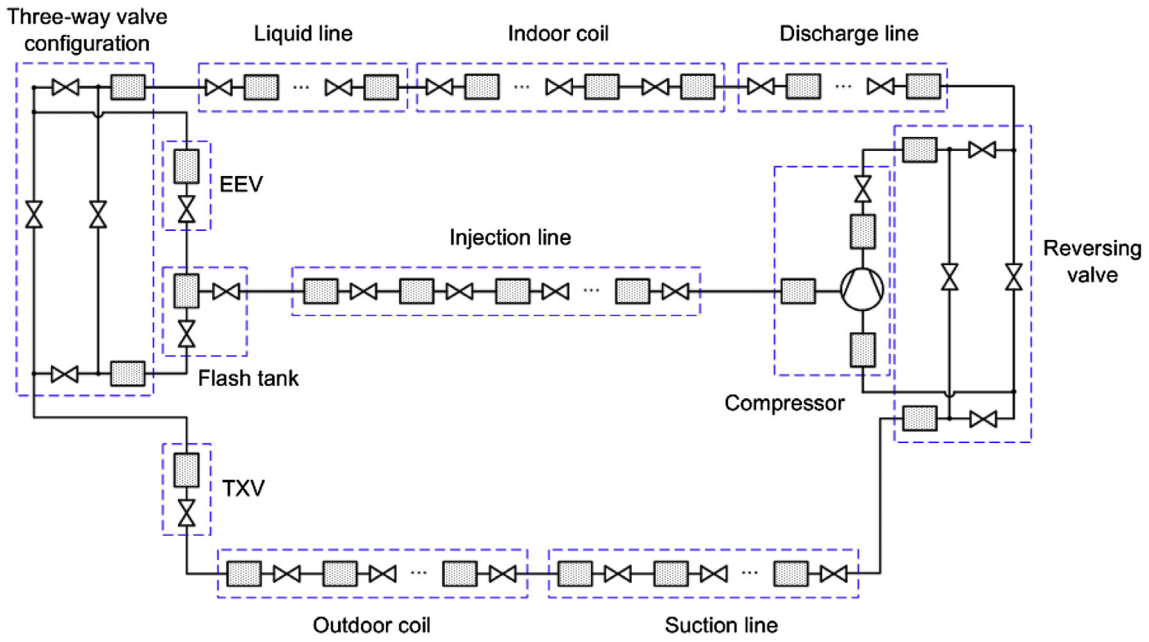

Fig. 9 – Model representation of the refrigerant side of FTVI system.

4. System model and implementation

4.1. *System model*

The system model is formed by combining all the component models (Fig. 9). The basic elements used to model the refrigerant flow are the control volume and the throttle. Each component model is comprised of a sequence of control volumes and throttles, and always begins with a control volume and ends with a throttle (Tummescheit, 2002). Mass and energy conservation is evaluated within the control volume, whereas the momentum conservation is solved using the throttle.

The inputs to each refrigerant control volume are defined as the inlet mass flow rate, the inlet refrigerant enthalpy, and the outlet mass flow rate, and the outputs are the time-varying pressure and enthalpy of the control volume. The inputs to the throttle are the pressure difference across the throttle and the inlet enthalpy of the flow, and the output is the mass flow rate through the throttle. Thus, the output of the throttle is an input to the next downstream control volume, whereas the outputs of the control volume serve as the inputs to the intermediate throttle. Therefore, each component model has the same boundary conditions, i.e. the inlet mass flow rate, the inlet refrigerant enthalpy, and the outlet pressure. The modular nature of the component models allows flexibility in the system configuration. As a result, the component models can be seamlessly linked together in an arbitrary manner, regardless of whether they are the flow equipment, like compressors and valves, or the heat transfer equipment, like heat exchangers.

4.2. *Implementation*

The proposed transinet models are implemented using the Modelica modeling language and the Dymola 7.4 simulation environment. All the refrigerant properties are evaluated using in-house curve-fitted property routines, developed based on the REFPROP 9.0 database (Lemmon et al., 2010). Empirical correlations are used to calculate the heat transfer coefficients and the pressure drops on both refrigerant side and air side in the models for heat exchangers and pipes (Table 3).

5. Conclusions

A first-principles transient model has been developed for FTVI system which employs a vapor injection scroll compressor.

Table 3 – Correlation summary.

Air side	
Heat transfer	
Forced convection – dry condition	Wang et al. (1999)
Forced convection – wet condition	Wang et al. (2000)
Natural convection	Churchill-Chu (1975)
Pressure drop	
Forced convection – dry condition	Wang et al. (1999)
Forced convection – wet condition	Wang et al. (2000)
Single-phase	
Heat transfer	Gnielinski (1976)
Pressure drop	Blasius (Incropera and DeWitt, 1996)
Two-phase (condensation)	
Heat transfer	Shah (1979)
Pressure drop	Lockhart-Martinelli (1949)
Two-phase (evaporation)	
Heat transfer	Kandlikar (1990)
Pressure drop	Grönnerud (1979)
Void fraction	Smith (1969)

The highlights of the modeling approach are summarized as follows:

(1) The vapor injection scroll compressor is modeled using a lumped parameter approach. The internal heat transfer between the refrigerant and metallic parts has been taken into account. The backflow phenomenon through the economizer port is handled carefully. The prevailing physics of the refrigerant during compressor "on" and "off" period are represented in the model.
(2) The heat exchangers are modeled using the segment-by-segment approach. The conditions for the fan "on" and "off" modes have been considered. A separated flow model without interfacial exchange is employed for two-phase flows to more accurately predict the refrigerant mass distribution. The method of "enthalpy correction" is proposed to account for the slip effect in two-phase flows.
(3) The flash tank is modeled as a lumped control volume with one inlet and two outlets. Ideal phase separation is assumed. All the possible scenarios of refrigerant state inside the tank have been considered (excluding the supercritical condition).
(4) The throttling portion of the electronic expansion valve and the thermostatic expansion valve is modeled using an empirical correlation, whereas the sensor bulb portion of the latter is modeled based on the energy balance.
(5) The reversing valve model is developed such that the same system model can be utilized to simulate both cooling and heating. This is particularly convenient when simulating system transients during reverse-cycle defrosting.
(6) The modular nature of the component models allows flexibility in the system configuration.

This paper only addresses the numerical modeling aspect. Transient simulations will be carried out for start-up and shut-down operations and a detailed comparison against the experimental data will be presented in Part II.

Acknowledgments

The authors wish to thank the support of the Integrated Systems Optimization Consortium of the Center for Environmental Energy Engineering at the University of Maryland.

REFERENCES

ASHRAE, 1998. Handbook – Refrigeration American Society of Heating, Refrigerating and Air-conditioning Engineers. Atlanta, U.S.A.

Baek, C., Lee, E., Kang, H., Kim, Y., 2008. Experimental study on the heating performance of a CO2 heat pump with gas injection. In: 12th International Refrigeration and Air Conditioning Conference at Purdue, West Lafayette, IN, USA.

Baroczy, C.J., 1965. Correlation of liquid fraction in two-phase flow with applications to liquid metals. Chem. Eng. Prog. S. Ser. 61, 179–191.

Bauer, O., 1999. Modeling of Two-phase Flows with Modelica. Master thesis. Lund Institute of Technology, Department of Automatic Control, Sweden.

Benapudi, S., Braun, J., 2002. A Review of Literature on Dynamic Models of Vapor Compression Equipment. ASHRAE Research Project 1043-RP.

Brasz, J.J., Koenig, K., 1983. Numerical methods for the transient behavior of two-phase flow heat transfer in evaporators and condensers. In: Shih, T.M. (Ed.), Numerical Properties and Methodologies in Heat Transfer. Springer Verlag, Berlin, pp. 461–476.

Butterworth, D., 1975. A comparison of some void-fraction relationships for cocurrent gas-liquid flow. Int. J. Multiph. Flow. 1 (6), 845–850.

Cho, H., Baek, C., Park, C., Kim, Y., 2009. Performance evaluation of a two-stage CO_2 cycle with gas injection in the cooling mode operation. Int. J. Refrigeration 32, 40–46.

Choi, J.W., Lee, G., Kim, M.S., 2011. Numerical study on the steady state and transient performance of a multi-type heat pump system. Int. J. Refrigeration 34 (2), 429–443.

Churchill, S.W., Chu, H.H.S., 1975. Correlating equations for laminar and turbulent free convection from a vertical plate. Int. J. Heat. Mass Transf. 18 (11), 1323–1329.

Cooper, M.G., 1984. Saturation nucleate pool boiling: a simple correlation. In: 1st U.K. National Conference on Heat Transfer, vol. 2, pp. 785–793.

Dittus, F.W., Boelter, L.M.K., 1985. Heat transfer in automobile radiators of the tubular type. Int. Commun. Heat. Mass Transf. 12 (1), 3–22.

Fu, L., Ding, G.L., Zhang, C.L., 2003. Dynamic simulation of air-to-water dual-mode heat pump with screw compressor. Appl. Therm. Eng. 23 (13), 1629–1645.

Gnielinski, V., 1976. New equations for heat and mass transfer in turbulent pipe and channel flow. Int. Chem. Eng. 16 (2), 359–368.

Grönnerud, R., 1979. Investigation of Liquid Hold-up, Flow-resistance and Heat Transfer in Circulation Type Evaporators, Part IV: Two-phase Flow Resistance in Boiling Refrigerants. Annexe 1972-1. Bull.. de l'Inst. du Froid, International Inst. of Refrigeration, Paris.

Gungor, K.E., Winterton, R.H.S., 1987. Simplified general correlation for saturated flow boiling and comparisons of correlations with data. Chem. Eng. Res. Des. 65, 148–156.

Haberschill, P., Gay, L., Auboin, P., Lallemand, M., 2003. Dynamic model of a vapour compression refrigerating machine using R-407C. HVAC&R Res. 9 (4), 451–466.

Hong, K.T., Webb, R.L., 1996. Calculation of fin efficiency for wet and dry fins. HVAC&R Res. 2 (1), 27–41.

Incropera, F.P., DeWitt, D.P., 1996. Introduction to Heat Transfer, third ed. John Wiley & Sons, New York.

Kandlikar, S.G., 1990. A general correlation for saturated two-phase flow boiling heat transfer inside horizontal and vertical tubes. J. Heat. Transf. ASME 112, 219–228.

Kærn, M.R., Elmegaard, B., Larsen, L.F.S., 2011. Experimental comparison of the dynamic evaporator response using homogeneous and slip flow modeling. In: Proceedings 8th Modelica Conference, Dresden, Germany, March 20–22, 2011.

Koury, R.N.N., Machado, L., Ismail, K.A.R., 2001. Numerical simulation of a variable speed refrigeration system. Int. J. Refrigeration 24 (2), 192–200.

Kuehn, T.H., Ramsey, J.W., Threlkeld, J.L., 1998. Thermal environmental Engineering, third ed. Prentice Hall, Upper Saddle River, New Jersey.

Lemmon, E.W., Huber, M.L., McLinden, M.O., 2010. NIST Reference Fluid Thermodynamic and Transport Properties – REFPROP Version 9.0. National Institute of Standard and Technology.

Levy, S., 1999. Two-phase Flow in Complex Systems. John Wiley & Sons, New York.

Lockhart, R.W., Martinelli, R.C., 1949. Proposed correlation of data for isothermal two-phase, two-component flow in pipes. Chem. Eng. Prog. S. Ser. 45, 39–48.
Ma, G.Y., Zhao, H.X., 2008. Experimental study of a heat pump system with flash-tank coupled with scroll compressor. Energy Build. 40, 697–701.
MacArthur, J.W., Grald, E.W., 1989. Unsteady two-phase compressible flow model for predicting cyclic heat pump performance and a comparison with experimental data. Int. J. Refrigeration 12, 29–41.
Mithraratne, P., Wijeysundera, N.E., Bong, T.Y., 2000. Dynamic simulation of a thermostatically controlled counter-flow evaporator. Int. J. Refrigeration 23 (3), 174–189.
Ndiaye, D., Bernier, M., 2010. Transient modeling of refrigerant-to-air fin-and-tube heat exchangers. HVAC&R Res. 16, 355–381.
Ploug-Sørensen, L., Fredsted, J.P., Willatzen, M., 1997. Improvements in modeling and simulation of refrigerant systems: aerospace tools applied to a domestic refrigerator. HVAC&R Res. 3 (4), 387–403.
Rasmussen, B.P., 2012. Dynamic modeling for vapor compression systems – Part I: literature review. HVAC&R Res. 18 (5), 934–955.
Scarcella, J. and Chen, Y.H., 2010. Liquid vapor separation in transcritical refrigerant cycle. Patent, No. WO2010039682A2.
Shah, M.M., 1979. A general correlation for heat transfer during film condensation inside pipes. Int. J. Heat. Mass Transf. 22, 547–556.
Smith, S.L., 1969. Void fraction in two-phase flow: a correlation based upon an equal velocity head model. Proc. Instn. Mech. Engrs 184 (36), 647–664.
Thome, J.R.S., 1964. Prediction of pressure drop during forced circulation boiling of water. Int. J. Heat. Mass Transf. 7, 709–724.
Tummescheit, H., 2002. Design and Implementation of Object-oriented Model Libraries Using Modelica. Ph.D. thesis. Department of Automatic Control, Lund Institute of Technology, Sweden.
Turner, J.M., 1966. Annular Two-phase Flow. Ph.D. thesis. Dartmouth College, Hanover, NH.
Umezu, K., Suma, S., 1984. Heat pump room air-conditioner using variable capacity compressor. ASHRAE Trans. 90, 335–349.
Wang, C.C., Lee, C.J., Chang, C.T., Lin, S.P., 1999. Heat transfer and friction correlation for compact louvered fin-and-tube heat exchangers. Int. J. Heat. Mass Transf. 42, 1945–1956.
Wang, C.C., Lin, Y.T., Lee, C.J., 2000. Heat and momentum transfer for compact louvered fin-and-tube heat exchangers in wet conditions. Int. J. Heat. Mass Transf. 43, 3443–3452.
Wang, X., Hwang, Y., Radermacher, R., 2009. Two-stage heat pump system with vapor-injected scroll compressor using R410A as a refrigerant. Int. J. Refrigeration 32, 1442–1451.
Winandy, E.L., Lebrun, J., 2002. Scroll compressors using gas and liquid injection: experimental analysis and modeling. Int. J. Refrigeration 25, 1143–1156.
Winkler, J., 2009. Development of a Component Based Simulation Tool for the Steady State and Transient Analysis of Vapor Compression Systems. Ph.D. thesis. Department of Mechanical Engineering, University of Maryland College Park, MD.
Xu, S., Ma, G., Liu, Q., Liu, Z., 2013a. Experiment study of an enhanced vapor injection refrigeration/heat pump system using R32. Int. J. Therm. Sci. 68, 103–109.
Xu, X., Hwang, Y., Radermacher, R., 2011a. Refrigerant injection for heat pumping/air conditioning systems: literature review and challenges discussions. Int. J. Refrigeration 34, 402–415.
Xu, X., Hwang, Y., Radermacher, R., 2011b. Transient and steady-state experimental investigation of flash tank vapor injection heat pump cycle control strategy. Int. J. Refrigeration 34, 1922–1933.
Xu, X., Hwang, Y., Radermacher, R., 2013b. Performance comparison of R410A and R32 in vapor injection cycles. Int. J. Refrigeration 36 (3), 892–903.
Zivi, S.M., 1964. Estimation of steady-state steam void-fraction by means of the principle of minimum entropy production. ASME Trans. J. Heat. Transf. 86, 247–252.